Secondary ion mass spectrometry and x-ray analysis of superconducting Nb/Pd multilayers

C. Gerardi,[a] M. A. Tagliente, A. Del Vecchio,[b] and L. Tapfer[c]
Centro Nazionale per la Ricerca e lo Sviluppo dei Materiali (PASTIS-CNRSM), Strada Statale 7 Appia km. 712, I-72100 Brindisi, Italy

C. Coccorese, C. Attanasio, L. V. Mercaldo, and L. Maritato
Dipartimento di Fisica, Università degli Studi di Salerno, I-84100 Salerno, Italy

J. M. Slaughter and C. M. Falco
Department of Physics, University of Arizona, Tucson, Arizona 85721

(Received 23 June 1999; accepted for publication 8 October 1999)

We report on accurate structural investigations of sputtered Nb/Pd multilayers by means of high-resolution secondary ion mass spectrometry and x-ray reflectivity. The combined use of secondary ion mass spectrometry and x-ray specular reflectivity techniques allows us to study the chemical configuration of the interfaces and to relate it to the observed superconducting properties. Secondary ion mass spectrometry analyses reveal a distinct Nb and Pd modulation and very sharp profiles with abrupt interfaces indicating a negligible interdiffusion of Nb and Pd at the interfaces. Moreover, analyzing the features in the Nb and Pd profiles and correlating them to the oxygen distribution in the multilayers and to the low-angle x-ray patterns, thin layers (3–4 nm thick) of niobium oxide were noticed at the Nb/Pd interfaces, while no oxide layers at the Pd/Nb interfaces could be detected. The role of this oxide layer in the determination of the crossover between three- and two-dimensional superconducting behavior in parallel external magnetic field, is discussed. © *2000 American Institute of Physics.* [S0021-8979(00)00902-6]

I. INTRODUCTION

The understanding of the interplay between superconductivity and low dimensional effects in periodic metallic multilayer structures is of great importance for the fabrication of new material structures exhibiting novel physical properties.[1] In fact, it is well known that in layered superconducting thin films with metallic spacers, such as in Nb/Pd or Nb/Cu material systems, the superconducting characteristics are modified by the proximity effect.[2–6]

Consequently, an accurate knowledge of the structural assessment and of the quality of the interfaces as well as the formation of interface layers (alloys and/or oxides) is crucial, due to the strong influence of the structural (roughness) and chemical properties of interfaces on the phase of the superconductive wave function in the interface region and, therefore, on the coupling between the closest superconductive layers.

In this work we investigate by highly depth-resolved secondary ion mass spectrometry (SIMS) and x-ray specular reflectivity (XSR) the structural properties of superlattices made of 10 periods, where each period is constituted by a thin niobium layer (superconductive material) separated by a palladium layer (spacer material).

We demonstrate that the combined use of SIMS and XSR is very effective for an accurate characterization of metallic superlattices (SL), allowing to determine the true layer thickness and to study both the interface quality and of the presence of very thin transition layers at interfaces. The precise determination of the superlattice period by XSR provides an internal standard, which allows one to calibrate the depth scale of the SIMS profiles and, hence, to measure the thickness of the single layers. In addition, XSR is a very powerful tool to control the thickness ratio between the single layers and to reveal any variation of the SL period and layer thickness ratio within the multilayered structure. In fact, it should be mentioned that due to sputter induced surface topography effects, which are enhanced in metal matrices,[7–10] SIMS profiles suffer from resolution degradation at higher depths.

Furthermore, XSR allows to study the surface and interface corrugations that influence the shape of the experimental patterns,[11] while the possible formation of oxide layers at the interfaces can be detected by SIMS using a low energy cesium beam and detecting OCs^+ molecular clusters. The formation of a thin niobium–oxide layer at the interfaces is in agreement with XSR results. In fact, only the presence of a thin NbO layer at the Nb/Pd interface allows one to obtain a satisfactory simulation of the experimental x-ray specular reflectivity patterns.[12] These results, with the presence of an oxide layer only at the Nb/Pd interface but not at the Pd/Nb one, are used to interpret the magnetic measurements and in particular to discuss the three- to two-dimensional crossover in the superconducting behavior of layered systems in parallel external magnetic field.

[a]Present address: ST Microelectronics, Strada Primosole 50, 95121 Catania, Italy.
[b]Present address: CIRA, via Maiorise, 81043 Capua (CE), Italy.
[c]Author to whom correspondence should be addressed; electronic mail: tapfer@cnrsm.it

II. EXPERIMENTAL DETAILS

A. Sample preparation

Nb/Pd multilayers were deposited on to Si(100) substrates using a magnetically enhanced dc triode sputtering gun for Pd and a magnetic gun for Nb, allowing the substrate holder to alternately pass over the targets.[13] The pressure in the sputtering chamber before the deposition process was typically in the low 10^{-7} Torr range and the Nb and Pd deposition rates were, respectively, about 90 and 2 Å/s. The nominal Nb layer thickness for all SL is about 18 nm, while the Pd layer thickness is different for each SL varying from 1.7 to 17 nm. Each superlattice is composed of ten Nb/Pd periods. In particular, the results of the structural characterization shown and discussed in this work, refer to two Nb/Pd superlattices, which are representative for all the investigated samples, with a nominal Pd layer thickness of 4 nm (sample A) and 8 nm (sample B), respectively. The first and the last layer of each sample was made of Pd in order to avoid surface superconductivity.

B. X-ray reflectivity measurements

Low-angle x-ray reflectivity analyses were performed with a single-axis diffractometer optimized for glancing-angle measurements and by using Cu $K\alpha$ radiation. The angular divergence of the incident beam in the diffraction plane is 0.03°. A parallel plate collimator and a graphite monochromator, placed between the sample and the proportional x-ray counter, collimate the diffracted x-ray beam and reduce the background intensity. In addition, high-angle θ–2θ x-ray diffraction measurements were performed in order to identify the phases in the constituent layers and to determine the preferred crystallographic orientation. High-angle x-ray diffraction measurements were carried out with a Philips PW1880 powder diffractometer equipped with a Cu x-ray tube (3 kW generator). The scans were performed in the 2θ angular range 5°–100° and with an angular step size of 0.02°.

C. SIMS measurements

SIMS analyses were performed with a CAMECA *ims4f* instrument by using either O_2^+ or Cs^+ primary ions. For the two beams, the energy and the angle of incidence were fixed to 1.8 keV (900 eV/O), 60° and 5.5 keV 42°, respectively. The primary beam was raster scanned over an area of 250 $\times 250\,\mu m^2$ with a current ranging from 20 to 50 nA. To avoid crater edge effects and problems arising from eventual rounding of the crater bottom observed especially in the case of the low energy oxygen beam, the secondary ions were collected from a circular aperture with a diameter of 8 μm centered on the sputtered area. The ion detection was carried out by two operating modes according to whether the primary ions were oxygen or cesium. Under oxygen bombardment we recorded the positive secondary ions Pd^+ and Nb^+. When a cesium beam was used, the molecular ions $NbCs^+$, $PdCs^+$, and OCs^+ were detected. The cesium cluster mode, usually employed to decrease the detrimental influences of matrix effects on the secondary ion yields,[14] allows us to increase the depth resolution and to detect the oxygen distribution throughout the structure.

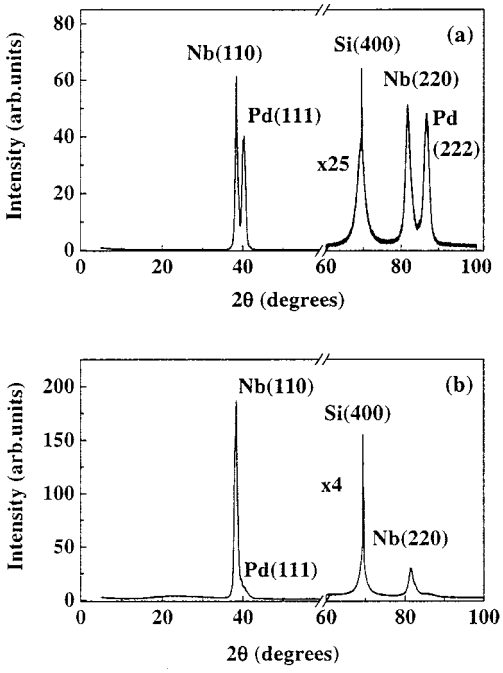

FIG. 1. High-angle diffraction patterns of sample *A* (curve *a*) and sample *B* (curve *b*). The spectra show the (400) Si substrate peak and the preferred (*hh*0) Nb and (*hhh*) Pd diffraction peaks.

D. Superconducting measurements

The H_{c2} measurements for both the perpendicular and parallel orientation of the magnetic field with respect to the plane of the films were performed on patterned samples with length $l=100\,\mu$m and width $w=15\,\mu$m, obtained by photolithographic technique and chemical etching, using a diluted hot solution of HF and HNO_3, with an etching rate of about 100 Å/s.

The H_{c2} values were measured at half of the resistive transition, whose width was less than 0.1 K in zero magnetic field. The external magnetic field was obtained with a superconducting solenoid able to reach 4 T at 4.2 K.

III. RESULTS AND DISCUSSION

A. X-ray scattering results

Figure 1 shows the high-angle diffraction patterns of the two investigated superlattices. The peaks corresponding to the Nb(110) and Nb(220) reflection can be clearly noted. The observation of the only ($hh0$) peaks clearly indicates that the Nb layers are of high crystallographic orientation and of well-defined crystal thickness. For the two samples, the crystal coherence length for the Nb layer was calculated to be about 11 nm (sample A) and 9 nm (sample B). In both cases, the coherence length is smaller than the nominal Nb thickness value as determined from x-ray specular reflectivity measurements. The x-ray spectra reveal that the Pd layers present a well-ordered structure and a preferred [111]-orientation for the superlattice with high Pd content [Fig.

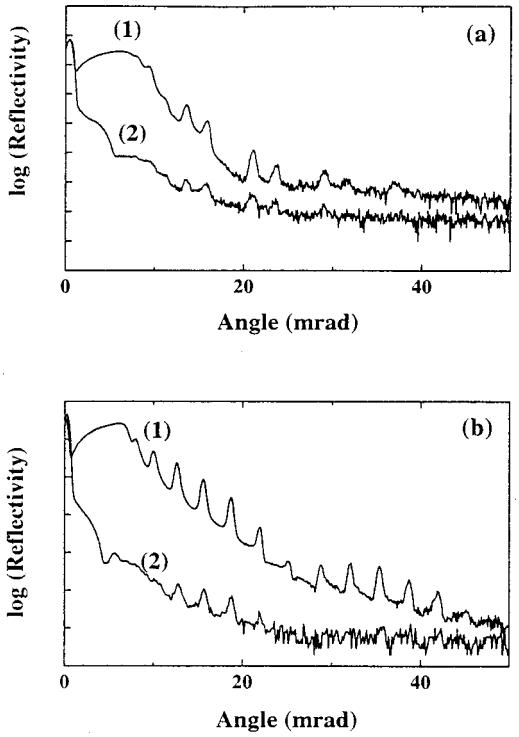

FIG. 2. Low-angle specular (1) and off-specular (2) 0.15° offset angle scans from the *A* (curve *a*) and *B* (curve *b*) Nb/Pd multilayers. Distinct satellite peaks due to the superlattice periodicity are observed.

1(a)]. In the other superlattice, the Pd(111) phase cannot be clearly identified (only a tail at the high angle side of the Nb(110) peak can be observed), since the x-ray scattering power is reduced due to the smaller layer thickness. It should be noted, that the x-ray patterns do not show, within the instrumental sensitivity, peaks originating from other crystallographic phases.

Figure 2 shows the low-angle reflectivity results as recorded in specular [curve (1)] and off-specular [curve (2)] geometry of the two samples under examination. In the off-specular measurements, the sample is offset from the specular condition by an angle of 0.15°. From the angular spacing between diffraction peaks which is correlated to the periodicity of the structure, we derived the multilayer period. The values calculated for the two superlattices were 27.4 nm (sample A) and 22.3 nm (sample B). Further indications are given by the presence of extinguished peaks at well defined positions and peak order which imply precise constant ratios between the thickness values of the alternating layers. In Fig. 2(a) the strong reduction of the specular component immediately after the critical angle ($\theta_c \approx 7$ mrad) indicates the presence of roughness at the surface and interfaces on the top of the sample.[15] In fact, since the x-ray penetration depth close to the critical angle is very small (1–4 nm) the scattered intensity comes from the top surface layers. At scattering angles $\theta \gg \theta_c$ the penetration depth increases and the scattered x-ray intensity from subsurface layers is revealed. Our scattering curves show, that the higher order peaks are well pronounced and, therefore, we can conclude that the internal interfaces may be smoother.

Off-specular measurements [curve (2) in Fig. 2] are performed in order to investigate the kind of roughness at different interfaces.[15] In the case of correlated (or conformal) roughness the diffuse scattering is localized at the satellite peak position, i.e., a periodicity of the intensity distribution (as in the specular condition) can be clearly observed and the diffuse scattering between the satellite peaks is reduced. On the contrary for uncorrelated interface roughness the diffuse scattering is uniformly distributed and no pronounced peaks can be observed. Our experimental data on both samples show that the diffuse intensity is partially localized near the satellite peaks and this clearly indicates that the roughness between the interfaces is correlated or partially correlated. This finding is also demonstrated from low-angle reciprocal maps (not reported here, see Ref. 16) which have shown the presence of correlated or partially correlated roughness between the interfaces.[11,15]

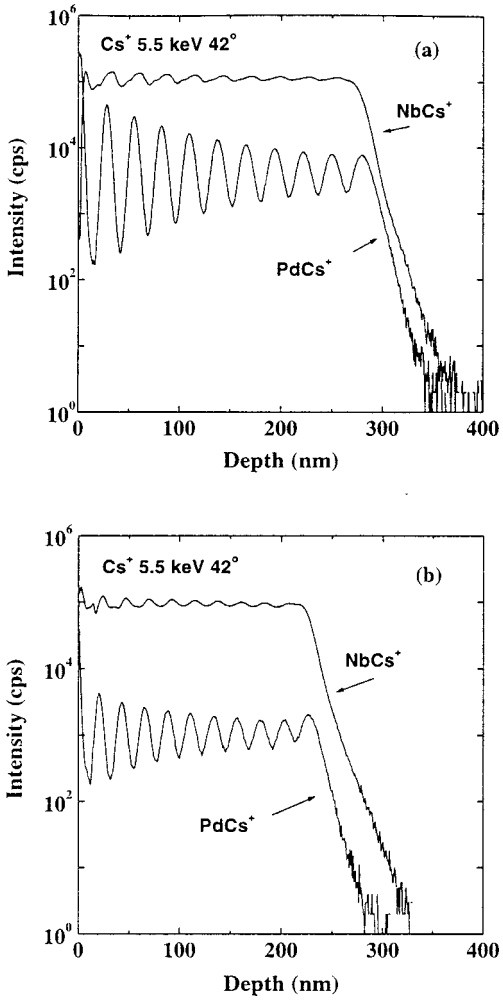

FIG. 3. MCs+ SIMS profiles of Nb and Pd, recorded under Cs^+, 5.5 keV, 42° conditions, of the two Nb–Pd superlattices in Figs. 1 and 2. The modulation of the $NbCs^+$ and $PdCs^+$ signals clearly indicate the periodic alternating layer sequence.

B. SIMS results

Figure 3 shows the $PdCs^+$ and $NbCs^+$ SIMS profiles of the two investigated superlattices. The periodic modulation of the Nb and Pd content through the ten periods of the superlattices is clearly observed. Highly depth-resolved

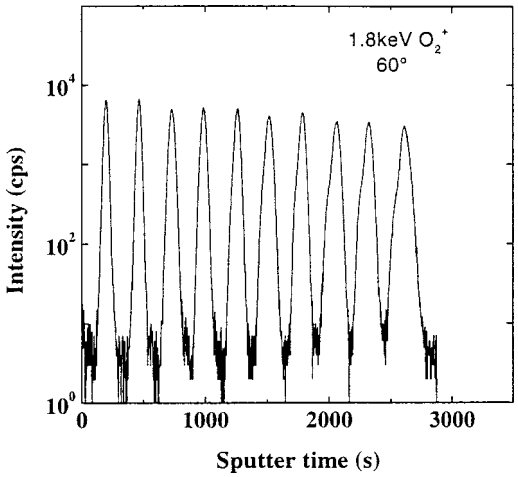

FIG. 4. SIMS depth profile of Pd, recorded under high-resolution conditions by using a 1.8 keV O_2^+ beam impacting at 60° the surface of sample *A*, calibrated by taking into account the period measured by XSR.

SIMS raw profiles of Nb and Pd, recorded by using the 1.8 keV O_2^+ (0.9 keV/O^+) beam, is shown in Fig. 4. In fact, the very low primary beam energy and the grazing incidence reduce the collisional effects and hence minimize the profile distortions allowing us to achieve highly depth-resolved profiles.[17]

SIMS profiles were calibrated taking into account the period measured by XSR. This parameter has been accurately determined and used as internal reference parameter for the calibration in Fig. 3. It should be noted, however, that the erosion speeds are different according to whether the beam sputters Nb or Pd matrix. To account for such differences we have measured, under identical experimental conditions, the erosion rates on both thicker reference targets. The resulting erosion rates are consistent with the ratio of the theoretical erosion rates obtained by calculating the sputtering yields of Nb and Pd by means of the Sigmund theory.[18]

Figure 5(a) shows the Pd and Nb profiles of the first periods, by using the 1.8 keV O_2^+ beam, after that the corrections for the difference of erosion speeds have been taken into account in the depth calibration. The thickness of Pd layers approximately derived from the full width at half maximum (FWHM) values of SIMS signals is of 6.6 nm. The presence of double peaks in the Nb signal can be observed in corresponding to the interfaces with the Pd layers. In these regions the Nb signal increases above the intensity corresponding to the pure Nb layers. These features are likely due to the presence of oxygen at the interfaces; the high oxygen content causes an increase of the Nb signal (matrix effect). This is more evident at the Nb/Pd interface with respect to the Pd/Nb interface as can be well observed in Fig. 5(b) where the Nb and Pd signals have been overlapped on a linear scale. During the sputter deposition the natural reactivity of niobium can very likely lead to the formation, especially at the Nb/Pd interface, of niobium oxide with a thickness of ~4 nm.

The less pronounced peak at the Pd/Nb interface is due either to a lower oxygen content in this region or to the fact that the oxide layer is very thin, below the SIMS depth resolution. It can be noted that the SIMS depth resolution degrades as the depth increases. This effect is frequently observed, especially for grazing angle incidence and very low energy primary beams, in sputter profiling, mainly due to the formation of sputter-induced surface topography.[17–21] In metal targets the degradation is enhanced by their polycrystalline nature.[7–10] It has been shown that the degradation can be reduced either under additional oxygen flooding during the analysis[22] or by using rotating sample holders.[9,23–25] As the depth resolution degrades, the apparent thickness of both Nb and Pd layers in SIMS profile increases. Figure 6 shows the variation of the Pd peak broadening, expressed in FWHM values with the depth. This is a clear depth-resolution artifact, because the XSR results show that the thickness of the layers is kept constant throughout the structure.

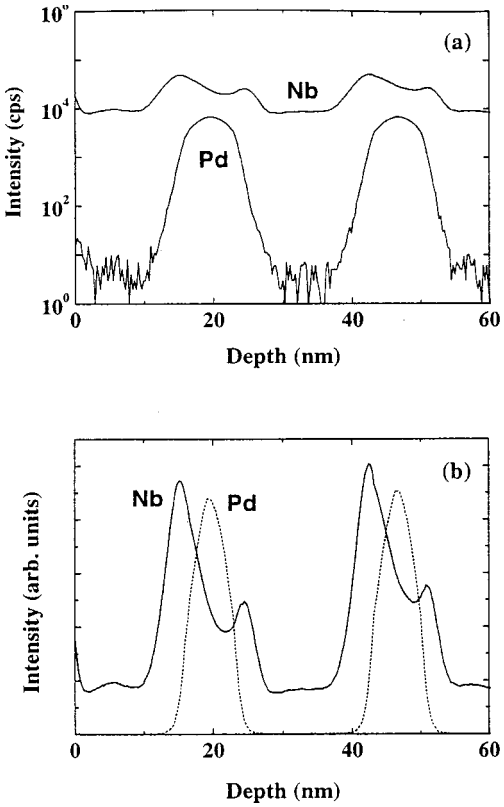

FIG. 5. SIMS depth profiles by using a 1.8 keV O_2^+ beam of the first two Nb/Pd stacks obtained from Fig. 4 after the corrections for the differences in erosion rates. The curves represent the intensity vs depth in semilogarithmic scale (a) and in linear scale (b). The locations of the matrix effect peaks on both the interfaces with the Pd layer are shown.

Assuming that in the falloff region the SIMS signal has an exponential behavior, we have measured for the first layers on the Pd signal a leading and trailing edge decay length of 0.75 and 0.79 nm, respectively. These good depth-resolution results demonstrate excellent instrumental performances as well as good interfaces exhibiting low interdiffusion effects. The good resolution is preserved within the first 100 nm and degrades at higher depths due to topography development during the sputtering process.

As mentioned above the peaks exhibited by the niobium signal at the interface with the Pd layers can be correlated to the probable formation of Nb oxide due to the presence of a

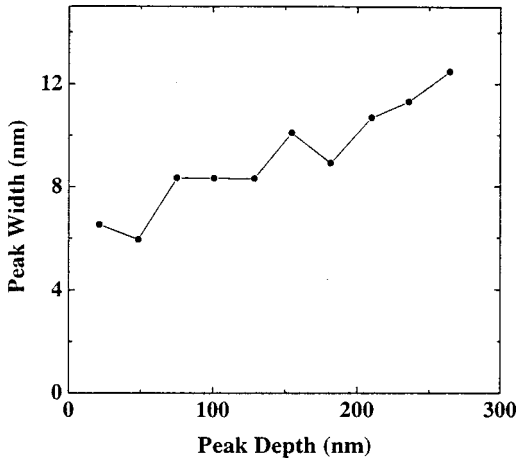

FIG. 6. Degradation of the SIMS depth resolution in the profile obtained under O_2^+, 1.8 keV, 60°, recorded as the enlargement with the depth of the FWHMs of the Pd peaks.

residual oxygen pressure in the sputter deposition chamber and the natural reactivity of the niobium. This deduction is confirmed by Fig. 7 which reports the Pd, Nb, and O profiles obtained by detecting the MCs^+ molecular ions. This is the best depth resolution which can be achieved by our instrument in the case of oxygen profiling. The figure shows that a large amount of oxygen is present in the region where the occurrence of peaks in the Nb signal was previously observed in Fig. 5. Unfortunately due to the higher primary energy used under the cesium bombardment (5.5 keV) the depth resolution obtained in Fig. 7 is not comparable with the one obtained in Fig. 5. In addition, an increased shift between the signals, corresponding to the different projected ranges of the implanted primary species in the distinct matrices can be observed in Fig. 7. This effect is enhanced by the higher energy of the impacting beam. Combining the results of Figs. 5 and 7, we concluded that niobium oxide layers with a thickness of about 4 nm are likely formed at the interface between the Nb and the Pd layers.

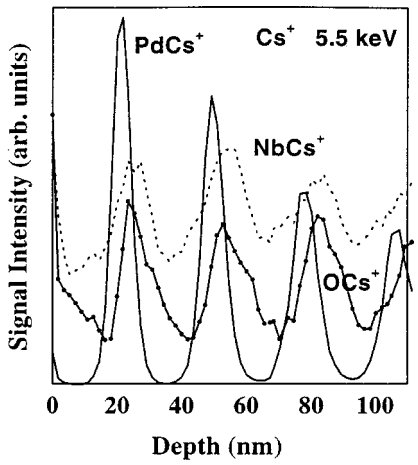

FIG. 7. MCs^+ SIMS profiles of Nb (dashed line), Pd (solid line), and O (dotted–solid line), recorded under Cs^+, 5.5 keV, 42° conditions.

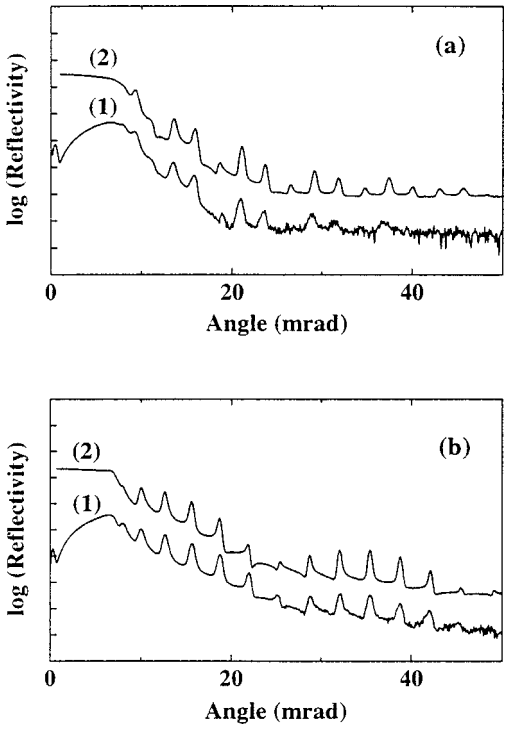

FIG. 8. Experimental (1) and calculated (2) low-angle true specular reflectivity scans from sample A (a) and B (b).

C. Simulation of the x-ray specular patterns

The experimental x-ray reflectivity patterns were calculated by using a theoretical model[12] for the specular intensity from nonideal multilayers which includes the interface roughness and roughness correlation. The calculations have been made with the assumption of the presence of a Nb–oxide layer at the Nb/Pb interface and a rms roughness distribution which varies linearly from the substrate to the surface.[16] In particular, we assume that the rms roughness varies linearly from the substrate to the multilayer surface in accordance with the relation

$$\sigma_j = \langle \sigma \rangle + \Delta\sigma \left(\frac{1-2j}{2(M+1)} \right).$$

Here, $\langle \sigma \rangle$ is the average rms roughness value, M is the stack number and $j = 1,...,M$. From the simulations we obtain that $\Delta\sigma = 1.0$ nm for sample A, while for the other sample we have $\Delta\sigma = 0.2$ nm. We have assumed that the interfacial Nb–O compound is a mixture of different kinds of Nb–oxides with an average atomic density corresponding approximately to the NbO phase. For both samples considered, the Nb–oxide layer was found to be 3 nm thick. Figure 8 shows excellent agreement between the experimental low-angle x-ray reflectivity and the simulated patterns. The parameters used for the simulations are summarized in Table I.

D. Superconducting properties

From the point of view of the superconducting properties, the Nb/Pd layered system is very interesting. In fact, Pd is a spin fluctuation metal which in principle could act as a very weak ferromagnet in depressing the critical temperature

TABLE I. Structural parameters obtained from the simulation of the experimental x-ray reflectivity patterns of the two considered multilayers. Here Λ_{SL} is the superlattice period and t_{Nb}, t_{Pd}, and t_{NbO} are the average thickness values of the Nb, Pd, and NbO layers, respectively. The rms roughness varies linearly around an average rms roughness $\langle\sigma\rangle$ over a range $\Delta\sigma$.

Sample	Λ_{SL}(nm)	t_{Nb}(nm)	t_{Pd}(nm)	t_{NbO}(nm)	$\langle\sigma\rangle$(nm)	$\Delta\sigma$(nm)
A	27.4	14.9	9.5	3	0.5	1
B	22.3	16	3.3	3	0.4	0.2

of the layered system. A similar situation, intermediate between the case of superconductor/normal metal multilayers[26] and that of superconductor/ferromagnetic system,[27] has been observed, for example, in Nb/CuMn multilayers,[28] in which the metallic spin glass CuMn layers can be treated as a weak ferromagnet. Previous measurements, performed on sputtered[13] and MBE grown[29] Nb/Pd multilayers, have shown a behavior of the critical temperature T_c vs the Pd layer thickness well described in terms of the deGennes–Werthamer theory[30] (see for example Fig. 4 in Ref. 29). This is also the case for the multilayers investigated in this work,[13] in which the T_c values scale well according to the proximity effect model.[30] From the deGennes–Werthamer theory, one can extrapolate, in the limit of very thin Pd layers, a critical temperature value of about 7.7 K, in good agreement with the T_c value of about 8 K measured on a single Nb film with an overall thickness of 200 nm obtained in the same sputtering conditions used to deposit the samples studied here. Such a low value of T_c could be related to the oxygen partial pressure present in the sputtering chamber during the deposition.

Figure 9 shows the $H_{c2\parallel}$ vs temperature curve for the Nb/Pd multilayers with Pd thickness of 1.7 nm (a), 6.6 nm (b), 13.2 nm (c), and 17 nm (d).

In superconducting multilayers, it is well known that, due to the temperature dependence of the superconducting perpendicular coherence length $\xi_\perp$, the parallel critical magnetic field $H_{c2\parallel}$ vs temperature curve goes from a linear dependence close to T_c to a square root like behavior at lower temperatures.[26] According to a Josephson coupling model,[31] this crossover should occur when $\xi_\perp/\Lambda = 0.7$, where Λ is the thickness of the modulation period. In short, this model could be applied only in the case of superconducting/insulating (SIS) multilayers. In the case of superconducting/normal metal (SNS) multilayers, only normal metal thickness of the order of 100 nm,[32] should give rise to this crossover effect. On the other hand, the 3D–2D crossover has been observed in a large number of SNS multilayers in the ranges of normal layer thickness of few tens of nanometers.[31] For the superlattices investigated in this study, the effect is clearly present for the multilayers with Pd thickness ranging from 1.7 to 17 nm as shown in Fig. 9. As also seen from the values of the anisotropic Ginzburg–Landau mass ratio,[13] these samples are strongly coupled superconducting layered systems well far from the weak coupling condition related to the Josephson effect.

From the discussion of the structural analyses in the previous sections, it is clear that the presence of the crossover effect in the $H_{c2\parallel}(T)$ curves of our samples could be related to the Nb oxide layers present on the top of each Nb layer. A similar explanation can also be proposed for the other Nb based SNS multilayers obtained by sputtering.[26]

Figure 10 reports the values of the $\xi_\perp(T)/\Lambda$ ratio versus the thickness of the nonsuperconducting layer. Using the parallel coherence length values and the anisotropic mass ratios in Ref. 27, the $\xi_\perp(T)$ are calculated at the crossover temperature defined as the temperature at which the behavior of the $H_{c2\parallel}(T)$ curves changes from linear to square-root-like. The theoretical value of 0.7 is approached in the limit of thin nonsuperconducting layers, while for large thickness of the Pd layers the obtained values are lower than 0.7. The presence of the Nb oxide on the top of the Nb layers plays an increasing role in the limit of thin Pd layers, rendering the

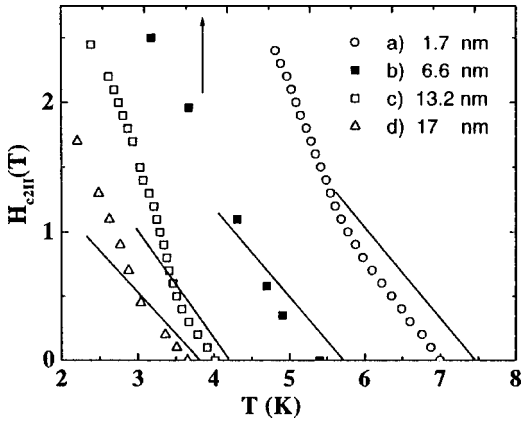

FIG. 9. The $H_{c2\parallel}$ vs temperature curves for the samples with Pd thickness of 1.7 nm (curve *a*), 6.6 nm (curve *b*), 13.2 nm (curve *c*), and 17 nm (curve *d*). It is possible to note a linear dependence for temperatures close to T_c.

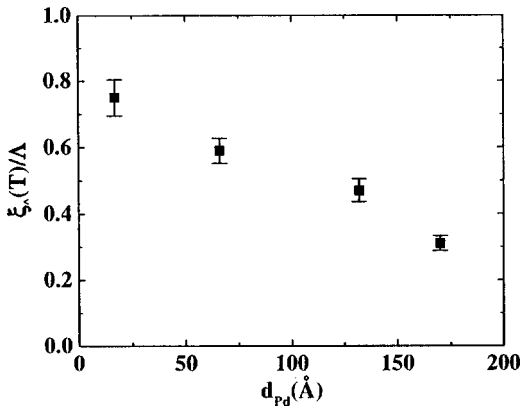

FIG. 10. The dependence of the $\xi_\perp(T)/\Lambda$ values calculated at the crossover temperatures vs the thickness of the Pd layers.

structure more SIS like, while in the case of thicker Pd layers the behavior of the system is strongly influenced by the tunneling through the metallic spacer giving rise to a more complicated structure (SNIS type) with respect to the case of the simple Josephson model,[31] which could determine the lower values of the $\xi_{\perp}(T)/\Lambda$ ratios.

Other models[33] have been proposed to explain the observed crossover in the $H_{c2\|}(T)$ curves of anisotropic superconducting systems. We point out that, applying these models, the actual modulation period is doubled with respect to that of ideal samples with perfect interfaces, due to the presence of the Nb oxide only at the Nb/Pd interfaces.

IV. CONCLUSIONS

The combined use of SIMS and XSR analyses turns out to be very effective for the characterization of metallic multilayers, such as the Nb/Pd superlattices, employed in experiments aimed at the investigation of the interplay between superconductivity and reduced dimensionality effects.

The period measured by XSR is used as an internal reference for the depth scale calibration of SIMS profiles. Nevertheless, due to the big differences in the sputter yields, an accurate evaluation of the sputter rates in thicker Pd and Nb layers is necessary to avoid misleading results. Using very low energy ion beams, we achieved a high initial depth resolution which allows us to determine that the interfaces exhibit negligible interdiffusion effects. The leading and trailing decay lengths of the Pd signal are of 0.75 and 0.79 nm, respectively. The good depth resolution is preserved in the first 100 nm then it degrades drastically due to surface topography development induced by the sputtering. Furthermore, SIMS analyses show that a large amount of oxygen is confined at the interface between Pd and Nb layers suggesting the formation of an interface oxide compound which is very likely due to the presence of residual oxygen in the growth chamber and the high reactivity of niobium. This result is confirmed by XSR measurements whose diffraction patterns can be explained only taking into account the presence of a NbO interface layer.

The presence of this Nb oxide on the top of each Nb layer can explain the presence of the 3D–2D crossover in the $H_{c2\|}(T)$ curves of our multilayers even at very small thickness of the Pd layers. Other data present in the literature, about Nb based sputtered multilayers[26] can be tentatively interpreted in terms of the presence of such an oxide layer. Here it is interesting to mention, that preliminary SIMS and XRD analysis on Nb/Pd structures grown by molecular beam epitaxy (MBE) in UHV environment, and consequently with a very low residual oxygen contamination in the growth chamber do not show the presence of a Nb oxide layer at the interface and no reduced matrix effect in the Nb signal of the SIMS measurements.

ACKNOWLEDGMENTS

The authors thank A. Cappello and A. Sacchetti for their valuable technical support in SIMS and XSR measurements, respectively.

[1] D. B. McWhan, *Synthetically Modulated Structures*, edited by L. L. Chang and B. C. Giessen (Academic, New York, 1985), Chap. 2.
[2] Q. S. Yang, C. M. Falco, and I. K. Schuller, Phys. Rev. B **27**, 3867 (1983).
[3] W. P. Lowe and T. H. Geballe, Phys. Rev. B **29**, 4961 (1984).
[4] J. Guimpel, M. E. De La Cruz, F. De La Cruz, O. Laborde, and J. C. Villegier, J. Low Temp. Phys. **63**, 151 (1986).
[5] J. M. Triscone, D. Ariosa, M. G. Karkut, and O. Fisher, Phys. Rev. B **35**, 3238 (1987).
[6] L. Maritato, A. M. Cucolo, R. Vaglio, C. Noce, J. L. Makous, and C. M. Falco, Phys. Rev. B **38**, 12917 (1988).
[7] R. G. Wilson, F. A. Stevie, and C. W. Magee, *Secondary Ion Mass Spectrometry* (Wiley, New York, 1989), p. 4.2-1.
[8] R. Stuck and J. PonPon, *Proceedings of Secondary Ion Mass Spectrometry, SIMS VI*, edited by A. Benninghoven, A. M. Huber and H. W. Werner (Wiley, New York, 1988), p. 507.
[9] A. Zalar, Thin Solid Films **124**, 223 (1985).
[10] W. Pamler and K. Wangemann, Surf. Interface Anal. **18**, 52 (1992).
[11] D. E. Savage, J. Kleiner, N. Schimke, Y. H. Phang, T. Jankowski, J. Jacobs, R. Kariotis, and M. G. Lagally, J. Appl. Phys. **69**, 1411 (1991).
[12] A. P. Payne and B. M. Clemens, Phys. Rev. B **47**, 2289 (1993).
[13] C. Coccorese, C. Attanasio, L. V. Mercaldo, M. Salvato, L. Maritato, J. M. Slaughter, C. M. Falco, S. L. Prischepa, and B. I. Ivlev, Phys. Rev. B **57**, 7922 (1998).
[14] Y. Gao, J. Appl. Phys. **64**, 3760 (1988).
[15] H. Zabel, Appl. Phys. A: Solids Surf. **58**, 159 (1994).
[16] M. A. Tagliente, A. Del Vecchio, L. Tapfer, C. Coccorese, L. Mercaldo, L. Maritato, J. M. Slaugther, and C. M. Falco, Nuovo Cimento **19**, 473 (1997).
[17] K. Wittmaack, Surf. Interface Anal. **21**, 323 (1994).
[18] P. Sigmund, in *Sputtering by Particle Bombardment I*, edited by I. R. Behrish (Springer, New York, 1981), Chap. 2.
[19] E.-H. Cirlin, J. J. Vajo, and T. C. Hasemberg, J. Vac. Sci. Technol. B **12**, 268 (1994).
[20] E. A. Eklund, R. Bruinsma, J. Rudnick, and R. S. Williams, Phys. Rev. Lett. **67**, 1759 (1991).
[21] E. Darque-Ceretti, M. Aucouturier, and A. Boutry-Forveille, Surf. Interface Anal. **18**, 229 (1992).
[22] J. C. Dupuy, C. Dubois, G. Prudon, R. Breiner, and P. Thevenard, Nucl. Instrum. Methods Phys. Res. B **64**, 636 (1992).
[23] S. Hofmann and A. Zalar, Surf. Interface Anal. **21**, 304 (1994).
[24] E.-H. Cirlin and J. J. Vajo, *Proceedings of Secondary Ion Mass Spectrometry, SIMS VIII*, edited by A. Benninghoven, K. T. F. Janssen, J. Tumpner, and H. W. Werner (Wiley, Chichester, 1992), p. 347.
[25] F. A. Stevie, P. M. Kahora, J. L. Moore, and R. G. Wilson, *Proceedings of Secondary Ion Mass Spectrometry, SIMS VIII*, edited by A. Benninghoven, K. T. F. Janssen, J. Tumpner, and H. W. Werner (Wiley, Chichester, 1992), p. 327.
[26] I. Banerjee, Q. S. Yang, C. M. Falco, and I. K. Schuller, Phys. Rev. B **28**, 5037 (1983); K. Kanoda, H. Mazaki, T. Yamada, N. Hosoito, and T. Shinjo, *ibid.* **33**, 2052 (1986); J. P. Loquet, Wsavenhans, Y. Bruynseraede, H. Homma, and I. K. Schuller, IEEE Trans. Magn. **MAG-23**, 1393 (1987); V. I. Dediu, V. V. Kabanov, and A. S. Sidorenko, Phys. Rev. B **49**, 4027 (1994).
[27] H. K. Wong, B. Y. Jin, H. Q. Yang, J. B. Ketterson, and J. E. Hilliard, J. Low Temp. Phys. **63**, 307 (1986); P. Koorevaar, Y. Suzuki, R. Coehoorn, and J. Aarts, Phys. Rev. B **49**, 441 (1994); S. Jang, D. Davidovic, D. H. Reich, and C. L. Chien, Phys. Rev. Lett. **74**, 314 (1995); Th. Muhge, N. N. Garifyanov, Yu. V. Goryunov, G. G. Khaliullin, L. R. Tagirov, K. Westerholt, I. A. Garifullin, and H. Zabel, *ibid.* **77**, 1857 (1996).
[28] L. V. Mercaldo, C. Attanasio, C. Coccorese, L. Maritato, S. L. Prischepa, and M. Salvato, Phys. Rev. B **53**, 14040 (1996); C. Attanasio, C. Coccorese, L. V. Mercaldo, S. L. Prischepa, M. Salvato, and L. Maritato, *ibid.* **57**, 14411 (1998).
[29] S. Kaneko, U. Hiller, J. M. Slaughter, C. M. Falco, C. Coccorese, and L. Maritato, Phys. Rev. B **58**, 8229 (1998).
[30] P. G. deGennes and E. Guyon, Phys. Lett. **3**, 168 (1963); N. R. Werthamer, Phys. Rev. **132**, 2440 (1963).
[31] R. A. Klemm, M. R. Beasley, and A. Luther, J. Low Temp. Phys. **16**, 607 (1974).
[32] J. Clarke, Proc. R. Soc. London, Ser. A **308**, 447 (1969).
[33] S. Takahashi and M. Tachiki, Phys. Rev. B **33**, 4620 (1986).